The flow generated in a continuously-stratified rotating fluid by the differential rotation of a plane horizontal disk

R. J. Munro * and P. A. Davies

Department of Civil Engineering, University of Dundee, Dundee DD1 4HN, UK

Abstract

Results are presented from a modelling investigation into the response of a rotating, linearly-stratified fluid to local forcing induced by a differentially rotating smooth, horizontal disk. Attention was directed at cases in which the disk forcing is relatively strong, with Rossby number $\varepsilon = \omega/2\Omega$ of order 1 or greater; here ω and Ω are the disk and background rotation frequencies respectively. The principal flow dynamics resulting in the mixing and deformation of the initially stable density distribution were identified as (i) shear-induced mixing due to the local increase in fluid vorticity above the disk and (ii) meridional circulations produced by Ekman processes and the constraint of the container sidewall. Laboratory experiments revealed the growth of a mixed layer adjacent to the disk and the subsequent development of layers within the mixed region. Furthermore, the experiments showed that, even at relatively large ε, Ekman processes associated with background rotation constituted the dominant mechanism controlling development and evolution of the primary interface between mixed and unmixed fluid regions. Theoretical, energy-based scalings are derived to describe the growth rate of the interfacial region for $\varepsilon \gtrsim \mathcal{O}(1)$ which are consistent with the $\varepsilon \to \infty$ limit corresponding to the $\Omega = 0$ case. These scalings are shown to describe well the development of the density field within the forced flow.

1 Introduction

Flow in a driven cavity is a topic of considerable research interest (see, for example, the review by Shankar & Deshpande, 2000) because of its wide importance in a number of industrial and environmental applications. The particular problem under investigation here, namely the response of a stratified,

* Email address: rick.munro@nottingham.ac.uk

contained fluid to impulsive surface forcing, has already an extensive scientific literature (Turner, 1973; Kato & Phillips, 1969; Scranton & Lindberg, 1983; Kantha *et al.*, 1977; Folse *et al.*, 1986; Folse & Wu, 1989; Chai & Kit, 1991; Fernando, 1991; Chai *et al.*, 1993; Davies *et al.*, 1995; Boyer *et al.* 1997) and the temporal and spatial development of the density field within the fluid is known to be complex.

The laboratory experiments to be described here constitute an extension of previous modelling investigations by Davies *et al.* (1995) on the flow generated by the rotation of a flat horizontal disk in a stably-stratified, initially-quiescent fluid. The present study considers the effects upon such a flow of introducing background rotation into the problem, not least in order to extend the range of applicability of the measurements to mixing processes in large lakes, reservoirs and oceanic basins where the background rotation of the Earth plays a dynamically significant role in determining the density structure and circulation of the surface wind-forced water body (Endoh *et al.*, 1990). The earlier laboratory studies by Davies *et al.* (1995) investigated cases in which the initial density stratification was linear and system rotation was absent and confirmed the three dimensional nature of the flow field generated by the disk motion. In addition, measurements of the interior density field demonstrated (i) the growth of a mixed layer above the disk and (ii) the development of staircase-like microstructure features in the initially-linear, vertical density profiles within the fluid body. Energy-based theoretical scalings for the growth of the mixed layer showed good agreement with the laboratory data but for the present cases, where the disk is rotating differentially within a system that is itself in uniform rotation, such scalings are expected to be invalid. This is primarily because of the particular importance of Ekman layer processes in the development of the velocity, vorticity and density fields within the differentially-rotating flow configuration (Spence *et al.*, 1992; Moulin & Flor, 2004). Such processes are considered here and the results are parameterized in terms of the strength of the external forcing, the initial density stratification and the background rotation.

2 Experiments

Fig. 1 shows the basic set-up of the experiment apparatus. The experiments were performed on a large rotating table, which could be rotated in either direction with angular velocity $\boldsymbol{\Omega} = \Omega \boldsymbol{e}_z$ ($\boldsymbol{e}_z$ denotes the unit vector along the axis of rotation; $\Omega \in [-0.6, 0.6]\,\mathrm{rad\,s^{-1}}$). An outer rectangular tank ($40\,\mathrm{cm} \times 40\,\mathrm{cm} \times 33\,\mathrm{cm}$), containing an inner cylindrical working tank (radius 18 cm, and depth 31 cm), was fixed to the top of the table so that the axis of the inner cylindrical tank was aligned along the rotation axis of the table. Connected to the base of the cylindrical tank was a smooth, flat horizontal disk (of radius

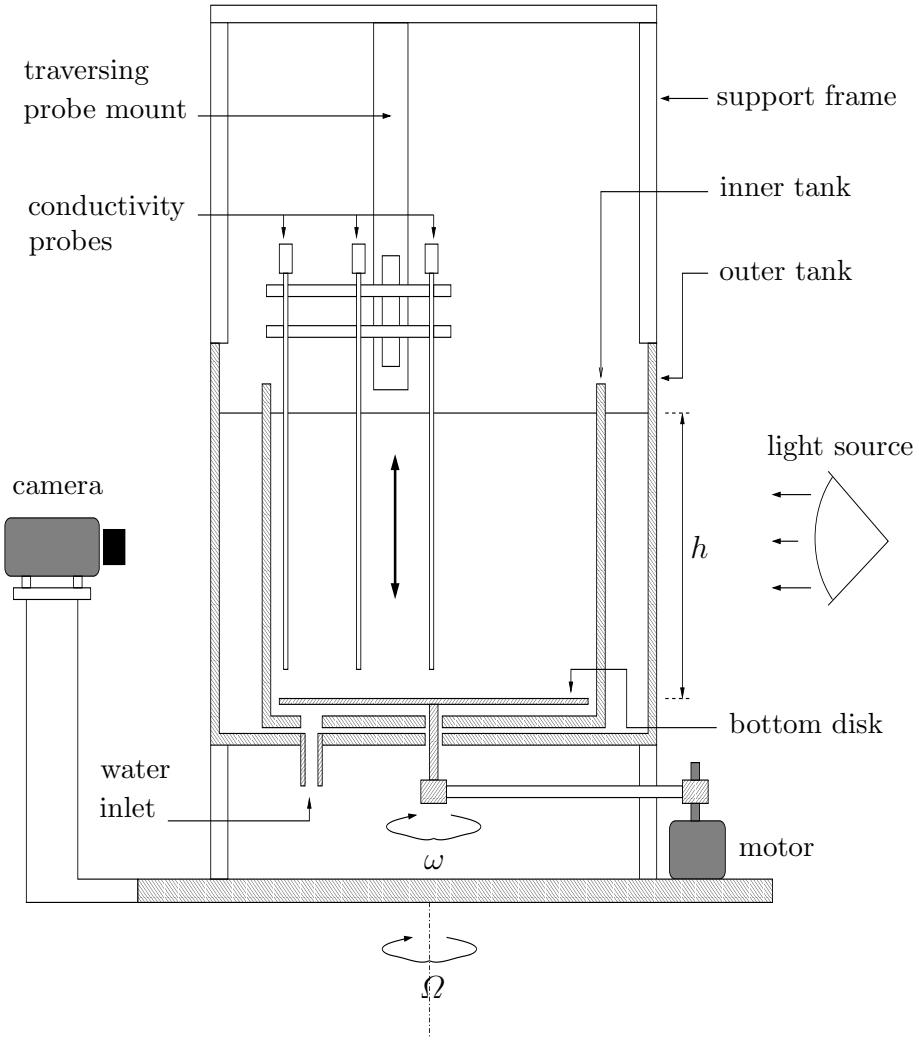

Fig. 1. Experimental apparatus.

$R_d = 17\,\mathrm{cm}$ and depth $0.5\,\mathrm{cm}$) which could be rotated independently of the table with angular velocity $\boldsymbol{\omega} = \omega \boldsymbol{e}_z$, with $\omega \in [0, 2]\,\mathrm{rad\,s^{-1}}$. (The gap between the disk edge and the vertical sidewall of the cylindrical container was $0.5\,\mathrm{cm} = 0.03R_d$, and had no significant affect on the flow dynamics.) Let (r, θ, z) denote the cylindrical coordinate system which rotates with constant angular velocity $\boldsymbol{\Omega} = \Omega \boldsymbol{e}_z$; as usual, z and r denote the vertical and radial coordinate directions respectively, with $z = 0$ corresponding to the disk surface, and the positive z-coordinate being aligned anti-parallel with the gravitational acceleration vector $\boldsymbol{g} = -g\boldsymbol{e}_z$.

The tanks were filled to a depth h, with a linearly salt-stratified water solution with initial stable density distribution of the form (Fortuin, 1960),

$$\rho(z) = \rho_0 + \frac{\Delta\rho}{h} z. \tag{1}$$

Here $\Delta\rho = \rho_h - \rho_0$, where ρ_0 and $\rho_h < \rho_0$ denote the values of ρ at $z = 0$

and $z = h$ respectively. Allowing a sufficient period after the filling process for the fluid to become quiescent, a measurement of the hydrostatic density profile was obtained. The table was then set in motion, with gradual increases in rotation rate being imposed until both the tank and the contained stratified fluid were in a state of solid-body rotation at the required frequency Ω. Once this state of rigid rotation was reached, the initial density profile was measured again, and used to calculate the initial buoyancy frequency, N_0, defined as,

$$N_0^2 = -\frac{g\Delta\rho}{\rho_0 h}. \tag{2}$$

Note that comparison between the hydrostatic density profiles and the corresponding profiles in the solid-rotation state showed no discernible differences. Of course, a state of purely static equilibrium cannot exist in this system (Greenspan, 1968) because of diffusive effects; however, for the experiments described in this article, with Froude number $Fr = \Omega^2 R_d/g \lesssim 10^{-2}$, the presence of any small-scale centrifugal convection will have negligible effect. See also Barcilon and Pedlosky (1967).

Measurements of the fluid density field were obtained using an array of three high-frequency response conductivity probes of the type developed by Head (1983). The probes were fitted to a vertical traverse mounted above the inner tank (see Fig. 1), and used to measure the vertical structure of the fluid density field (during the downward stroke only) over the range $0.04 \leqslant z/h \leqslant 0.96$, at radial locations $r/R_d = 0$, 0.5 and 0.9. A small motor was used to drive the sliding traverse, which was controlled, together with the acquisition and storage of conductivity and probe-height data, by a personal computer mounted on the rotating table. The time for a single traverse and the sampling frequency of the probes were approximately 1.5 s and 200 Hz respectively, which produced essentially instantaneous conductivity measurements every 0.08 cm. Each profile of conductivity data was converted to corresponding density measurements after the completion of each experiment. The correspondence between conductivity and density was established empirically using a simple calibration procedure, which was repeated and verified several times during the experiment campaign. It should be noted that the probe output is also dependent on the fluid temperature, and so care was taken to ensure that each experiment (and calibration) was performed only after a sufficient time period had elapsed to allow the fluid to reach the ambient temperature of the laboratory. To aid in the interpretation of the measured density profiles, images of the integrated density-perturbation field were also obtained during each experiment using the standard shadowgraph technique (Davies, 1992). The images were obtained using a digital video camera mounted on the table with the fluid illuminated using a standard slide projector directed horizontally through the opposite tank wall (see Fig. 1).

Once the initial measurements of the density field had been obtained, the disk

Table 1
Experiment details, listed in order of decreasing Rossby number, ε.

Experiment	Ω (rad s^{-1})	ω (rad s^{-1})	N_0 (rad s^{-1})	E ($\times 10^{-5}$)	ε	λ_1	λ_2
A	0.13	2.5	2.1	12.0	9.6	16.2	0.8
B	0.13	1.7	1.3	12.0	6.5	10.0	0.8
C	0.20	2.0	2.1	8.0	5.0	10.5	1.1
D	0.20	1.8	1.6	8.0	4.5	8.0	0.9
E	0.20	1.8	1.3	8.0	4.5	6.5	0.7
F	0.26	1.6	2.0	6.2	3.1	7.7	1.3
G	0.15	0.7	0.7	11.0	2.3	4.7	1.0
H	0.30	1.2	1.8	5.0	2.0	6.0	1.5
I	0.30	1.0	1.0	5.0	1.7	3.3	1.0

motion was initiated (at $t = 0$). The subsequent transient response of the system to the constant forcing induced by the disk rotation may be described conveniently in terms of the independent dimensionless dynamical, geometric and fluid-property parameters,

$$E = \frac{\nu}{\Omega h^2}, \quad \lambda_1 = \frac{N_0}{\Omega}, \quad \lambda_2 = \frac{N_0}{\omega}, \quad \eta = \frac{R_d}{h}, \quad \sigma = \frac{\nu}{\kappa_s}, \tag{3}$$

where ν is the kinematic viscosity of the fluid, and κ_s the molecular mass diffusivity of the stratifying agent (both assumed to be constant), with the Rossby and mid-disk Reynolds numbers defined as,

$$\varepsilon = \frac{\omega}{2\Omega} = \frac{\lambda_1}{2\lambda_2}, \quad Re_M = \frac{R_d^2 \omega}{4\nu} = \frac{\varepsilon \eta^2}{2E}. \tag{4}$$

In the experiments to be described, the dynamical quantities (Ω, ω, N_0) were varied, with the remaining geometric and fluid-property parameters (h, R_d, ν, κ) kept fixed throughout (with $\eta \approx 0.7$ and $\sigma \approx 700$). The relevant experiment details are given in Table 1. Before proceeding it is useful to define the spin-up time-scale, $\tau = E^{-\frac{1}{2}} N_0^{-1}$ (Spence *et al.*, 1992), the number of disk rotations, $n = \omega t / 2\pi$, and the vertical length scale $l_z = R_d \Omega / N_0$ (Moulin & Flór, 2004), which will be used in the following sections to describe the data. Attention was directed at cases in which the forcing of the flow was relatively strong; values of ε were of order unity or greater to facilitate comparisons with Davies *et al.* (1995).

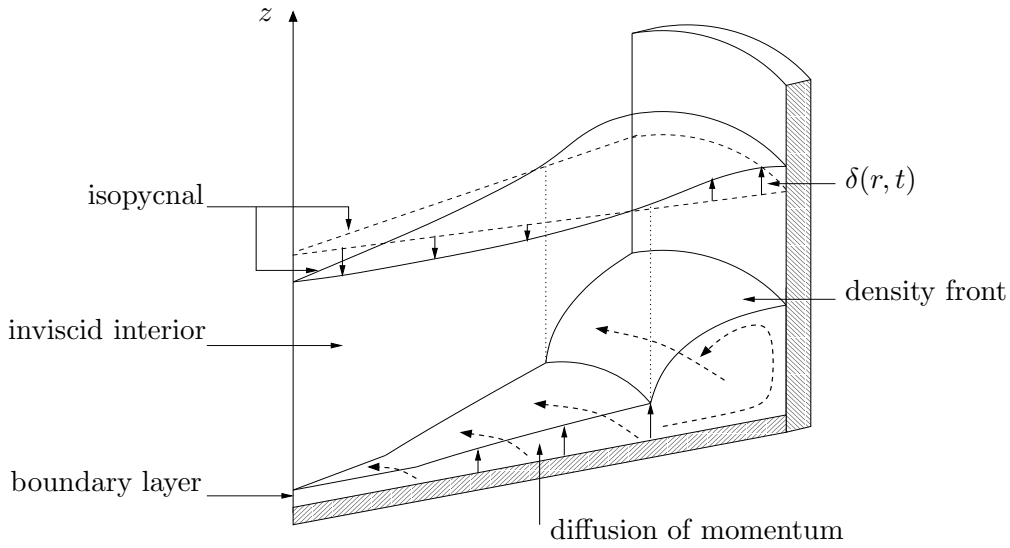

Fig. 2. Schematic diagram showing the important features of the initial flow, and the resulting effect (including the vertical isopycnal displacement $\delta(r,t)$ - see text) on the background stable density field.

3 Flow description

3.1 Initial flow development

The schematic in Fig. 2 illustrates the important features of the initial flow. When the disk is set in motion, the fluid above the disk is initially at rest relative to the rotating container. Within several disk rotation periods, a thin Ekman-type boundary layer has developed adjacent to the disk surface in which fluid particles are rapidly spun-up to the larger angular velocity by direct viscous action (Ekman, 1905). The increase in Coriolis acceleration is sufficient to overcome the radial pressure gradient along the disk and the layer-fluid is transported radially outwards (as well as azimuthally in the same direction as the disk), to be replaced by a vertical flux of fluid from the inviscid interior. For the case considered here (*i.e.*, that of relatively strong forcing induced by the disk motion), this circulation results in correspondingly large values of mid-disk Reynold's number (*e.g.*, for the experiments listed in Table 1, $Re_M \in [5, 13] \times 10^3$). Consequently, the induced boundary layer will be turbulent over most of the radial domain, resulting in enhanced levels of both momentum diffusion and mixing directly above the disk, at corresponding radial positions.

During the initial stages, the radial transport of fluid within the boundary layer is forced upwards by the container side-wall (at $r = R_d$, $z = 0$) into the inviscid interior where the fluid is relatively-lighter. This results in a localized adverse (radial and vertical) density gradient, causing the ejected layer-fluid, which has significant zonal velocity induced while in the boundary layer, to

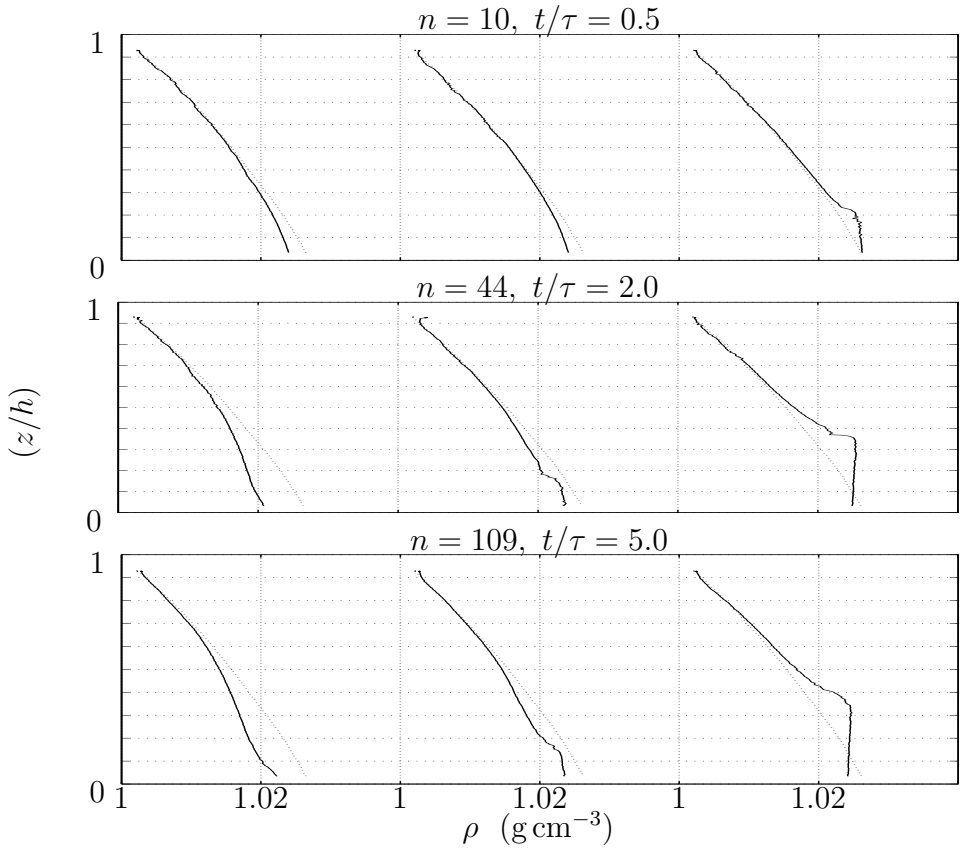

Fig. 3. Experiment I: sequence of density profiles during the early stages of the flow development, with $\tau \approx 140\,\mathrm{s}$ and $l_z \approx 5\,\mathrm{cm}$. Each sequence consists of the three profiles obtained at radial locations $r/R_d = 0,\ 0.5,\ 0.9$ (from left to right respectively); the corresponding initial linear profiles are also shown (dotted-lines). The horizontal density axis for the bottom plot is the same for the two above.

fall back down in a overturning meridional* circulation, resulting in the development of a density front in the corner regions (see Fig. 2). Furthermore, a strong vertical zonal shear is established at the interface between the developing density front and the interior undisturbed fluid, with corresponding values of localized Richardson number sufficiently low (Davies *et al.*, 1995) for Kelvin Helmholtz-type billows to form at this interfacial region, resulting in entrainment and interfacial mixing between the two regions.

The radial transport of fluid within the boundary layer induces a vertical velocity within the inviscid interior (Ekman-suction) which acts to stretch fluid columns and so increase the background cyclonic vorticity, to produce a downward deformation of the initial isopycnals. In contrast, following the formation of the density front, the isopycnals in the inviscid interior directly above the corner regions of the container are deformed vertically upwards, causing compression of the background vorticity. This process is illustrated in

* It is common when describing swirling flows to refer to the azimuthal velocity and (r, z)-plane as the zonal velocity and meridional plane respectively.

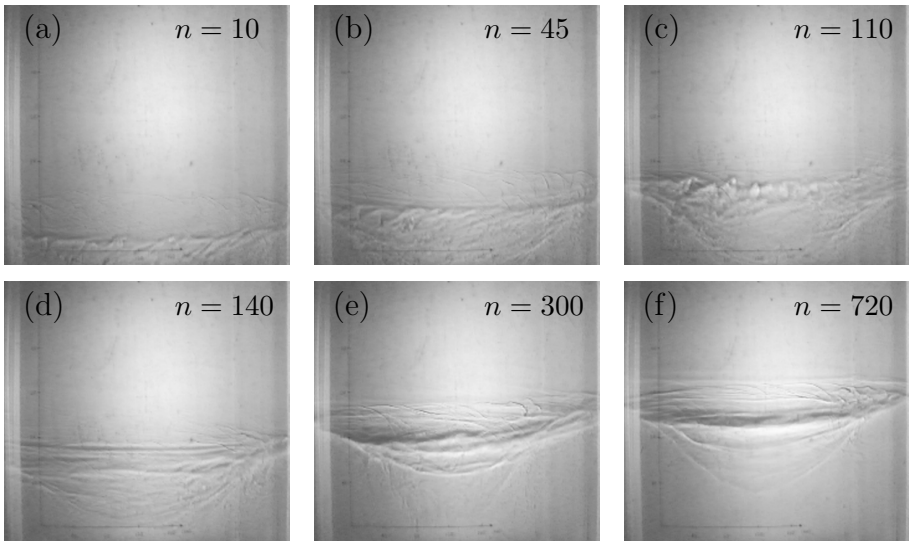

Fig. 4. Experiment I: sequence of shadowgraph images with the corresponding number of disk rotations, $n = \omega t/2\pi$, shown in the top right-hand corner of each image.

Fig. 2 where an initial isopycnal, prior to the onset of disk motion, is shown as the broken-line planar segment, and the corresponding deformed isopycnal in the current state represented by the solid-line surface (arrows are shown to illustrate the direction of deformation). Note how the maximum vertical displacement of the isopycnals, in the region where the background vorticity is stretched, is shown to occur at $r/R_d = 0$ (Moulin & Flór, 2004)[†]. (A detailed discussion of the isopycnal behaviour will be given in Section 3.3.)

Fig. 3 shows a sequence of measured density profiles from Experiment I, at radial locations $r/R_d = 0$, 0.5, 0.9, illustrating the development of the density field during the early stages of the flow. The initial linear profiles, corresponding to the solid rotation state, are shown, with the number of disk rotations, n, and corresponding dimensionless time, t/τ, indicated along the top of each plot. Fig. 4(a)-(c) shows a corresponding sequence of shadowgraph images taken at similar times. (The central, illuminated elliptical region in all images is an artifact of the illumination system and should be ignored here.)

The initial effects of the features described above can be observed in Fig. 3 after $n = 10$ disk rotations. At radii $r/R_d = 0$ and 0.5 the density profiles below $z/h \approx 0.5$, while remaining essentially linear, are deformed vertically

[†] Moulin & Flór (2004) analysed the transient response of a linearly-stratified fluid in a state of solid-rotation, to the local spin-up by a small horizontal rotating disk of radius much less than the lateral extent of the fluid. Hence, unlike the situation considered in this article, the ejected boundary-layer fluid is not confined by the presence of vertical boundaries, and is permitted to propagate radially outwards beyond the disk edge, as far as the Coriolis constraint will allow.

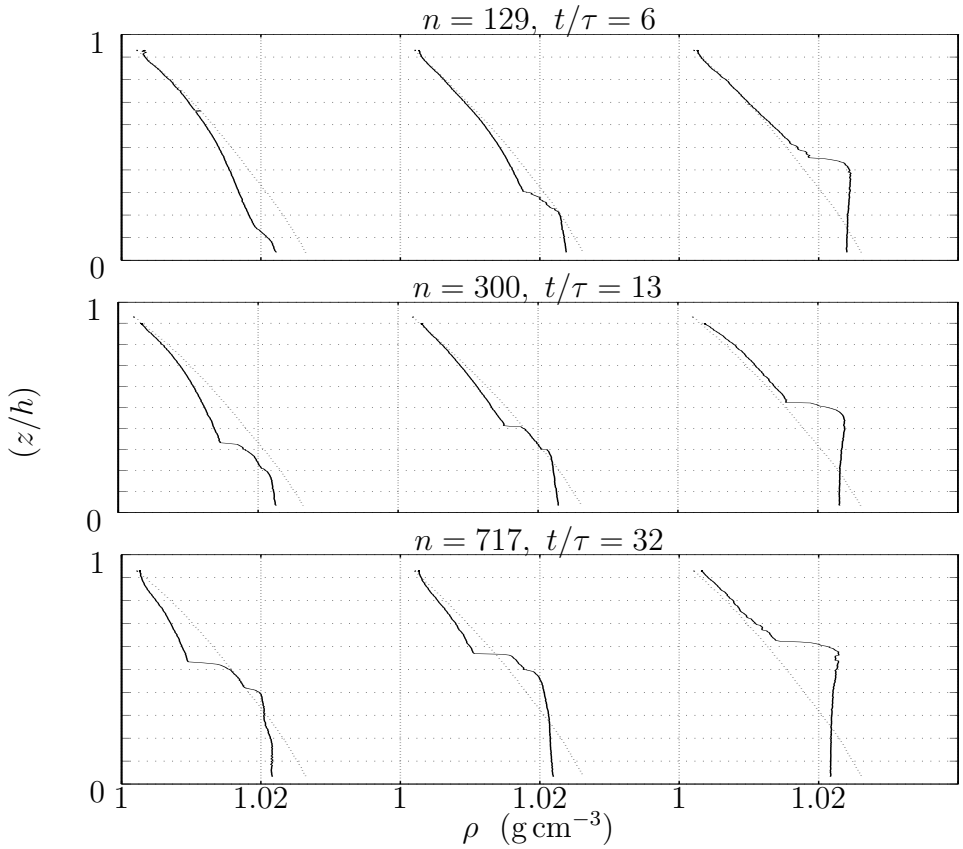

Fig. 5. Experiment I: sequence of density profiles during the later stages of the flow development. (The specific details of the above plots are given in the caption of Fig. 3.)

downward by Ekman suction, with maximum deformation occurring along the central axis $r/R_d = 0$. Likewise, the initial formation of the density front at the tank corner is observed (below $z/h \approx 0.25$) in the $r/R_d = 0.9$ profile. Note how at this stage the front consists of well-mixed fluid of uniform density ρ_0 (since the radial boundary-layer flux during these initial stages is of the heaviest available fluid), and how the profile above this region remains linear but is deformed vertically upwards. The corresponding profiles after $n = 44$ disk periods illustrate how the boundary layer continues to feed the density front with fluid from the base of the inviscid interior, the density of which is gradually decreasing from the initial value ρ_0. In particular, note how in the $r/R_d = 0.9$ profile, the density inside the well-mixed region (below $z/h \approx 0.4$) is now less than ρ_0 [‡]. This flux of relatively lighter fluid, coupled with the entrainment of lighter interior fluid across the interfacial region of the density front (described above), allows the vertical extent of the front-intrusion to

[‡] It is also worth highlighting the existence of the weak adverse vertical density gradient in the $r/R_d = 0.9$ profile, caused by the relatively lighter boundary-layer fluid entering the frontal region from below. The meridional and zonal motions that mix the frontal fluid ensure that this local component of density gradient remains weak, and so has no significant dynamical role.

increase gradually. Furthermore, the well-mixed heavier fluid contained within the recirculating density-front establishes a local radial density gradient across the interface, which, if large enough to overcome the restoring effect of the Coriolis force, can result in an increase in the radial extent of the front. The mixing induced by turbulent momentum diffusion from the disk surface is also now visible in the $r/R_d = 0.5$ profile, at the lower edge of the interior region below $z/h \approx 0.2$. Similarly, note how the density within this mixed region is less than the density within the corresponding well-mixed region of the density front at $r/R_d = 0.9$, again due to the radial flux of lighter fluid through the boundary layer. The downward deformation induced on the $r/R_d = 0$ density profile by Ekman suction is now considerable.

Further evidence of the features described above can be seen in the sequence of shadowgraph images[§] shown in Fig. 4. In particular, after $n = 10$ disk periods the initial development of the corner density front can be seen in the bottom section of the container. The wavy texture in the intensity field illustrates the low wavenumber components of the shear-induced turbulence that exists in this region, at this time. The images after $n = 45$ and $n = 110$ rotation periods show how the radial and vertical extent of the density front gradually increase, and illustrate that the recirculating fluid contained within the corner density front is well-mixed and essentially homogeneous. Also, note that in each of these images the interior fluid above the developing density front remains unmixed and linearly stratified.

3.2 Intermediate- and later-stages of the flow development

Fig. 5 shows a sequence measured of density profiles from Experiment I, during the intermediate- and later-stages of the flow development, with corresponding shadowgraph images shown in Fig. 4(d)-(f). As the processes described above continue, the boundary-layer transport coupled with restoring buoyancy forces and turbulent diffusion of momentum away from the disk surface, result in partially-mixed relatively-heavy fluid, originating at levels close to the disk surface, being overturned within the resulting meridional frontal circulation, and returned to the axis at $r/R_d = 0$ (Davies *et al.*, 1995). This overturned state can be seen clearly in the density profiles after $n = 129$ disk periods in Fig. 5, where there is now a mixed region in the $r/R_d = 0$ profile below $z/h \approx 0.15$. Evidence of the onset of this state is first observed in the $n = 109$ profiles of Fig. 3, by the occurrence of a density jump in the $r/R_d = 0$ profile. That is, comparison of the central profiles at $n = 44$ and $n = 109$ shows there

[§] The contrast variability evident in a shadowgraph image is associated with the variability in the second spatial derivative in the density field (Davies, 1992). Consequently, a region of uniform intensity in a shadowgraph image can correspond to either homogeneous or linearly-stratified density field.

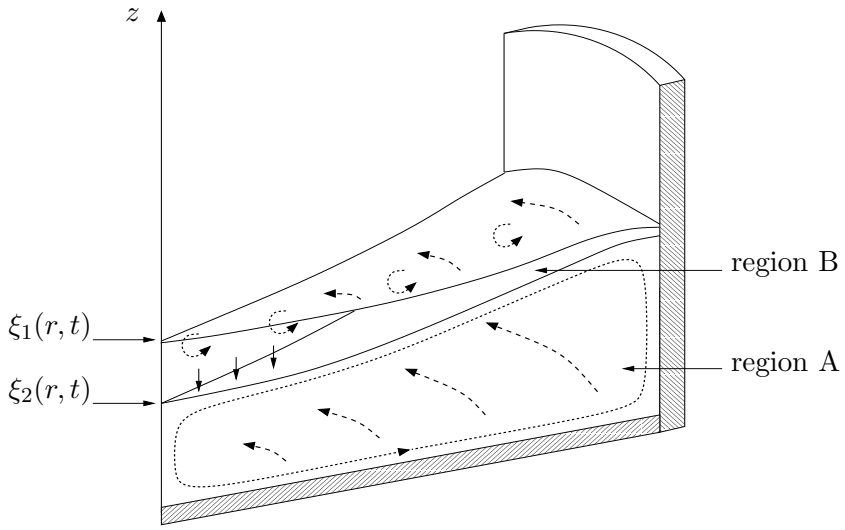

Fig. 6. Schematic diagram showing the important features of the flow after the development of the primary and secondary interfaces.

is an increase in density in the $n = 109$ profile below $z/h \approx 0.1$ (albeit, still less the original measured density at that corresponding level at $t = 0$).

Once the overturning event describe above has occurred, the density profiles at subsequent times can be characterized as consisting of two distinct regions separated by a continuous interface with a central depression. Namely, (a) an upper interior region in which the initially linear density field has been "stretched" (or "compressed", depending on radial position) by the effects of Ekman suction, but which shows no evidence of any mixing, and (b) a lower region adjacent to the disk surface consisting of a partially-mixed fluid. The interface separating these two distinct regions will henceforth be referred to as the *primary* interface, and denoted by $z = \xi_1(r,t)$; note that this notation is intended to imply that the interface may be regarded as being axisymmetric in nature. Fig. 6 illustrates the important features of the density-field structure during the later stages of the flow.

The fluid below the primary interface is now essentially in a state of solid rotation with angular velocity comparable with that of the disk, while a weaker azimuthal motion has diffused in to the unmixed fluid in the interior region above $\xi_1(r,t)$ [¶]. As a result, the significant zonal shear is now confined to a localized region about $\xi_1(r,t)$, but is reduced from that observed initially at the onset of disk motion. The shear is still sufficient to exhibit Kelvin Helmholtz-type billows, albeit with smaller amplitude. This effect is clearly evident in

[¶] This is a classical effect of a stable stratification on the spin-up of a rotating fluid, where buoyancy forces act to inhibit vertical motions. Consequently, there is a reduction in the ability of the Ekman layers to stretch the background vorticity (as a whole), and so viscous diffusion becomes an important mechanism in the spin-up of the interior fluid (Greenspan, 1968; Walin, 1969; Spence *et al.*, 1992).

the shadowgraph images in Fig. 4, by comparing the images after $n = 45$ and $n = 300$ disk periods. An inspection of the corresponding interfacial regions shows that the interface has a more smooth and regular texture at the later stage than initially observed, indicating a reduced level of interfacial mixing at the later stages of development.

A further consequence of the development of the primary interface is that the vertical flux of lighter interior fluid is no longer supplied directly to the sub-interfacial fluid adjacent to the disk surface. This region of relatively-heavy fluid is, however, still subject to the influence of the disk boundary-layer (provided there remains a vorticity deficit in this region of fluid, relative to the disk rotation frequency). Hence, the meridional recirculation that is established in this sub-interfacial region (by mechanisms already described) is no longer directly diluted by a flux of lighter interior fluid, as before. This results in the development of a density sub-structure beneath the primary interface, with the eventual formation of a secondary interface, $\xi_2(r,t)$, below which the fluid density becomes well-mixed by a dominant meridional circulation (region A, Fig. 6). In contrast, the fluid in the region $\xi_2 \leqslant z \leqslant \xi_1$ (region B, Fig. 6) is dominated by the significant interfacial shear and so remains partially-mixed (and stratified) due the entrainment of lighter interior fluid through the upper interface, $\xi_1(r,t)$.

The established secondary interface $\xi_2(r,t)$ is clearly evident in the measured profiles shown in Fig. 5 after $n = 300$ disk periods (at $z/h \approx 0.2, 0.3, 0.5$ in the respective radial profiles $r/R_d = 0, 0.5, 0.9$). The fluid below $\xi_2(r,t)$ is essentially well-mixed, with the density at $z/h = 0$ now approximately the same at each radial location (and obviously less than ρ_0). The significant levels of mixing are now confined to the region $\xi_1 \leqslant z \leqslant \xi_2$, where the degree of shear is greatest, whereas the fluid above $\xi_1(r,t)$ remains unmixed, only affected by the "stretching" (or "compression") of the background vortex. It is also worth highlighting the weak stratification that exists in the profiles at $r/R_d = 0, 0.5$ in the region below $\xi_2(r,t)$, due to the supply of relatively light fluid from the base of the region above $\xi_2(r,t)$, caused by the vertical flux induced by the disk boundary layer through Ekman suction. The important features described above can also be seen in the shadowgraph images shown in Fig. 4. In particular, note the primary interface just after detachment ($n = 130$), and the fully developed secondary interface during the different phases after $n = 300, 720$ disk rotations.

The processes described above continue, with (i) gradually decreasing shear-induced mixing confined to the region $\xi_1 \leqslant z \leqslant \xi_2$, and (ii) dilution of the region below $\xi_2(r,t)$ dominated by Ekman suction and the resulting meridional circulation. It is worth noting that in a number of the experiments listed in Table 1 a tertiary interface was observed, below $\xi_2(r,t)$, during the later-stages of the flow development (*e.g.*, Fig. 5, $n = 717$).

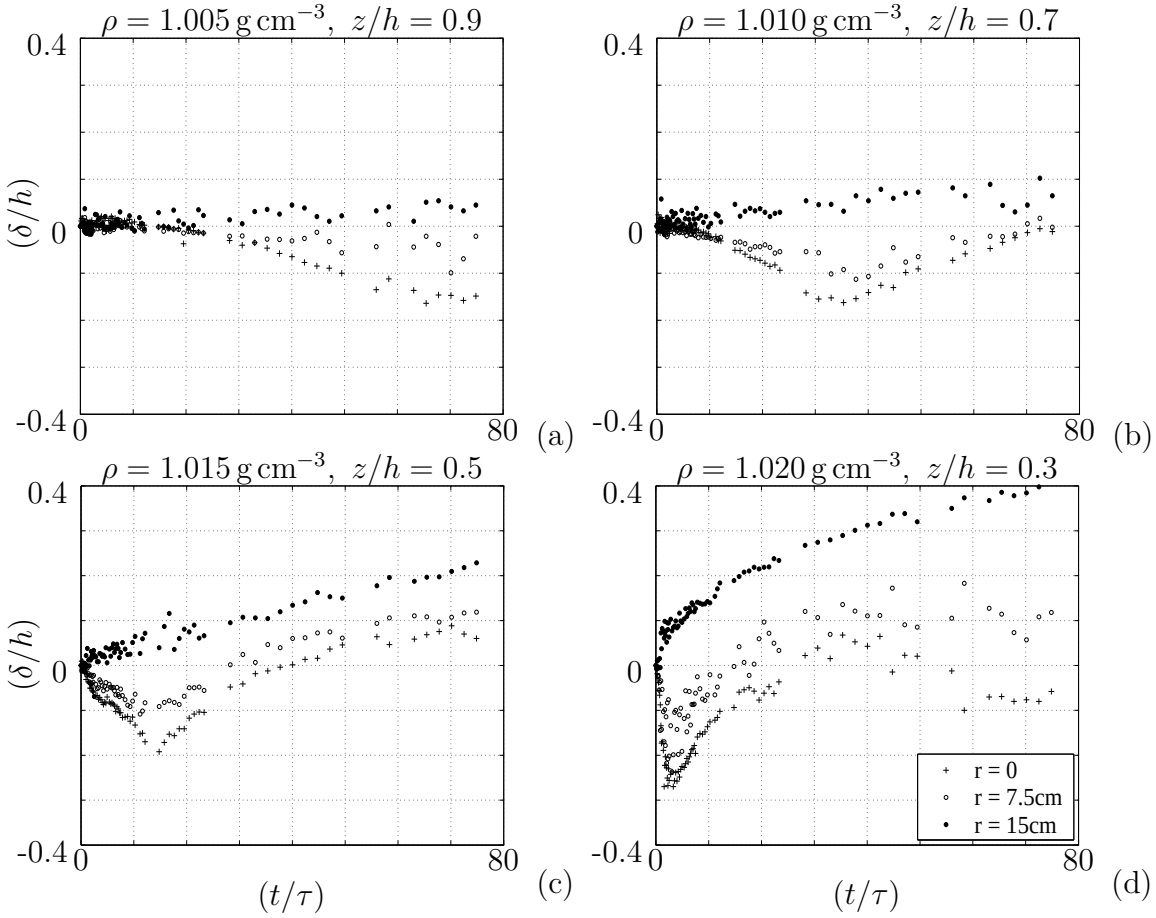

Fig. 7. Experiment I: plots showing the transient behaviour of the displacement, $\delta(r,t)$, of four separate isopycnals (the specific isopycnal density and corresponding initial height are shown along the top of each plot). Each plot contains three sets of measurements corresponding to the radial locations $r/R_d = 0,\ 0.5,\ 1$; $\delta(r,t)$ and t have been made dimensionless using h and $\tau = E^{-\frac{1}{2}}N_0^{-1}$ respectively.

3.3 Isopycnals

Additional features of the flow described above can be observed by analyzing how an initially-undisturbed isopycnal is deformed by the flow. At each radial location (where, for simplicity, axisymmetry is assumed), let $\delta(r,t;\rho)$ denote the vertical displacement experienced by a given isopycnal surface (of density ρ) about the initial state, as the flow develops; $\delta(r,t)$ is shown schematically in Fig. 2. Fig. 7 shows sequences of $\delta(r,t)$ obtained from the Experiment I density profiles, with each plot showing the behaviour of a different isopycnal at radial locations $r/R_d = 0,\ 0.5,\ 1$.

Consider first the sequences shown in Fig. 7(d), relating to the isopycnal initially closest to the disk surface at $z/h = 0.3$. At the onset of disk motion at $t = 0$ the isopycnal at $r/R_d = 0,\ 0.5$ is deformed downward by the induced vertical suction velocity, with maximum negative displacement observed along

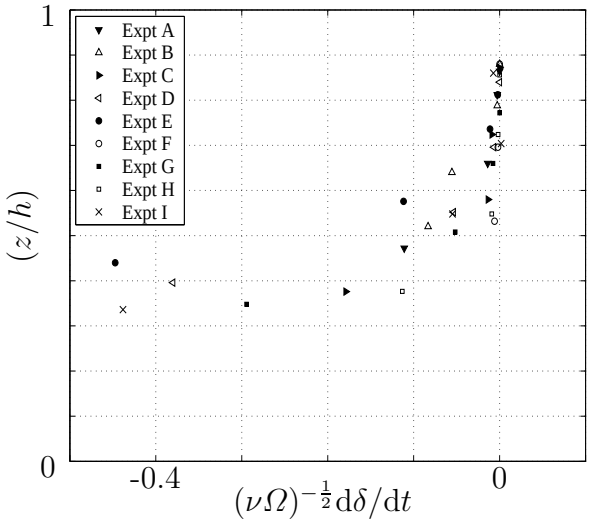

Fig. 8. Estimates for $(\nu\Omega)^{-\frac{1}{2}}\mathrm{d}\delta/\mathrm{d}t$ obtained from the $r/R_d = 0$ density profiles from each of the experiments in Table 1 at different heights z/h.

the central axis. Conversely, at $r/R_d = 1$, the isopycnal is deformed upward by the formation of the density front in the tank corner. This situation continues until $t/\tau \approx 5$, when there is a significant transition in the behaviour of $\delta(r,t)$ at $r/R_d = 0,\ 0.5$, as $\mathrm{d}\delta/\mathrm{d}t$ switches from being negative to positive. This transition corresponds to when the isopycnal has descended sufficiently to pass below the advancing (now formed) primary interface $\xi_1(r,t)$. Furthermore, formation of $\xi_1(r,t)$ corresponds to a change in the way the frontal fluid is supplied by the relatively-light interior fluid (*i.e.*, no longer directly through the disk boundary-layer). The consequences of this mechanistic change can be seen in the behaviour of $\mathrm{d}\delta/\mathrm{d}t$ at $r/R_d = 1$, where the relatively rapid displacement initially observed slows down and becomes essentially constant beyond $t/\tau > 5$. The period $5 < t/\tau < 30$, during which $\mathrm{d}\delta/\mathrm{d}t > 0$ at $r/R_d = 0,\ 0.5$, corresponds to when the $\rho = 1.02\,\mathrm{g\,cm^{-3}}$ isopycnal is located within region B, *i.e.* below $\xi_1(r,t)$ but above the secondary interface $\xi_2(r,t)$ (which becomes formed at $t/\tau \approx 10$); this is illustrated by inspection of the corresponding density profiles in Fig .5. Inside this stratified region B, the isopycnal follows the advance of $\xi_1(r,t)$ upward through the fluid and so $\mathrm{d}\delta/\mathrm{d}t$ remains positive. However, at $t/\tau \approx 30$, the isopycnal leaves region B and enters the essentially well-mixed fluid below $\xi_2(r,t)$, defined early as region A. (This is illustrated by inspection of the density profiles at $r/R_d = 0$ shown in Fig. 5, where at $t/\tau = 6$ the $\rho = 1.02\,\mathrm{g\,cm^{-3}}$ isopycnal is located below $\xi_1(r,t)$, and then at $t/\tau = 32$ where it is about to enter region A.) As the isopycnal enters region A there is a corresponding transition to $\mathrm{d}\delta/\mathrm{d}t < 0$ at $r/R_d = 0,\ 0.5$ due to the weak stratification that exists in region A at these radial locations (again, see Fig. 5). Eventually, as $\xi_1(r,t)$ advances vertically through the fluid, and the well-mixed fluid within region A is slowly diluted, the $\rho = 1.02\,\mathrm{g\,cm^{-3}}$ isopycnal ($> \rho_0 - \Delta\rho/2$) will cease to exist.

Consider now the remaining sequences shown in Fig. 7, relating to the isopycnals initially located at $z/h = 0.9$, 0.7, 0.5 respectively. The characteristics observed in these sequences are essentially the same as those described above, although, clearly, both the level of displacement observed and the rate at which it occurs are reduced the further the initial isopycnal is away from the disk surface. At $r/R_d = 0$, 0.5 both of the sequences shown in Fig. 7(b,c) still exhibit a local minima (*i.e.*, $\mathrm{d}\delta/\mathrm{d}t = 0$), at $t/\tau \approx 35$, 15 respectively, followed by a period where $\mathrm{d}\delta/\mathrm{d}t > 0$ corresponding to the times at which the respective isopycnal becomes located beneath the advancing interface $\xi_1(r,t)$. Also note, for the isopycnal initially situated at $z/h = 0.9$ (Fig. 7(a)), $\delta(r,t) \approx 0$ for $t/\tau < 20$, and it is not until $\xi_1(r,t)$ has advanced to height of order $h/2$ above the disk surface that any deformation is induced. This highlights how the differential in vorticity between the fluid above and below $\xi_1(r,t)$ (coupled with background rotation) is able to induce a significant vertical (Ekman-type) suction.

Finally, it is worth noting that during the initial stages of the flow, $\mathrm{d}\delta/\mathrm{d}t$ at $r/R_d = 0$ is proportional to the vertical suction velocity induced in the inviscid interior by the radial transport of fluid through the boundary layer. Analysis of each experiment showed that there exists an initial period (*e.g.*, $0 \leqslant t/\tau \leqslant 5$ for Experiment I) over which $\mathrm{d}\delta/\mathrm{d}t$ at $r/R_d = 0$ is essentially stationary, for which case one expects the appropriate scaling to be (Moulin & Flór, 2004),

$$\frac{\mathrm{d}\delta}{\mathrm{d}t} \sim (\nu\Omega)^{\frac{1}{2}} F\left(z/h; \varepsilon, \lambda_1, \lambda_2\right), \tag{5}$$

where F is a function of $\mathcal{O}(1)$. Fig. 8 shows estimates of $(\nu\Omega)^{-\frac{1}{2}}\mathrm{d}\delta/\mathrm{d}t$ during this quasi-stationary period, at different heights z/h, for each of the experiments in Table 1.

4 Parameterization for the growth rate of $\xi_1(r,t)$

In this section a simple model for the growth rate of the primary interface $\xi_1(r,t)$ is derived, based on estimates of energy conservations in the flow. The model relates specifically to the experiments described in this article for which $\varepsilon \sim \mathcal{O}(1)$, where both disk motion and background rotation are relevant to the flow dynamics. This basic model is then extended by considering the limit of large ε and how the flow dynamics are affected as $\Omega \to 0$, with ω kept fixed and of order $1\,\mathrm{rad\,s^{-1}}$, with corresponding modifications to the model proposed. Finally, the opposite limiting case of $0 < \varepsilon \ll 1$ is also briefly discussed by considering how the corresponding energy scalings are affected in the limit $\omega \to 0$ (where, similarly, 2Ω is kept fixed and of order $1\,\mathrm{rad\,s^{-1}}$), and the background rotation is the dominant mechanism.

Following Davies *et al.* (1995), the rate of work required to mix the fluid below the interfacial region, denoted by W_1, can be estimated by,

$$\frac{\mathrm{d}}{\mathrm{d}t}W_1 \sim \rho\, R_d^2\, N_0^2\, \xi^2\, \frac{\mathrm{d}\xi}{\mathrm{d}t}, \tag{6}$$

where $\xi(t)$ denotes the mean interfacial height defined by,

$$\xi(t)R_d = \int_0^{R_d} \mathrm{d}r\, \xi_1(r,t). \tag{7}$$

In section 3, the dominant flow features resulting in the formation of the primary interface were identified as the combined zonal and meridional motions due to turbulent momentum diffusion from the disk surface coupled with the Ekman dynamics induced by background rotation. Hence, taking $(R_d\omega, R_d\Omega)$ as the appropriate scales for zonal and meridional motions and Ω^{-1} as the relevant time scale, the rate of work input by the fluid, denoted by W_2, can be estimated by,

$$\frac{\mathrm{d}}{\mathrm{d}t}W_2 \sim \rho\, \omega\, \Omega^2 R_d^5. \tag{8}$$

Combining the expressions in (6) and (8), by assuming that a proportion of the input work is used to mix the fluid within the interfacial volume, gives the relationship,

$$\left(\xi^3/L^3\right) = k_1 \omega t, \tag{9}$$

where k_1 is a dimensionless proportionality coefficient and the length-scale L is given by,

$$L = R_d\, (\Omega/N_0)^{\frac{2}{3}} = R_d\, \lambda_1^{-\frac{2}{3}}. \tag{10}$$

Estimates for ξ^3/L^3, obtained from the measured density profiles for each of the experiments listed in Table 1, are plotted in Fig. 9(a) against number of disk periods, $n = \omega t/2\pi$; corresponding values of ε for each data set are shown in the legend. Over this $\mathcal{O}(1)$ Rossby number range the data accord well with the derived scaling given by (9) and (10), with the proportionality coefficient k_1 increasing monotonically with ε. A least-squares linear fit was applied to each of the scaled data shown in Fig. 9(a) to provide estimates for k_1 at each value of ε; the results of this procedure are shown in Fig. 9(b).

Davies *et al.* (1995) used a similar energy conservation argument to show that the appropriate scaling for the $\Omega = 0$ case (with ω of order $1\,\mathrm{rad\,s^{-1}}$), can be expressed as (9) with the corresponding length-scale L given by,

$$L = R_d\, (\omega/N_0)^{\frac{2}{3}} = R_d \lambda_2^{-\frac{2}{3}}. \tag{11}$$

Hence, for the case $\varepsilon \gg 1$, where the flow dynamics are completely dominated by the motions induced by the disk rotation and characterized by $(R_d\omega, \omega^{-1})$, the interface growth can be scaled using (9) with L given by (11). However, in the transition from (11) to (10), corresponding to $\varepsilon \to \mathcal{O}(1)$ (from above),

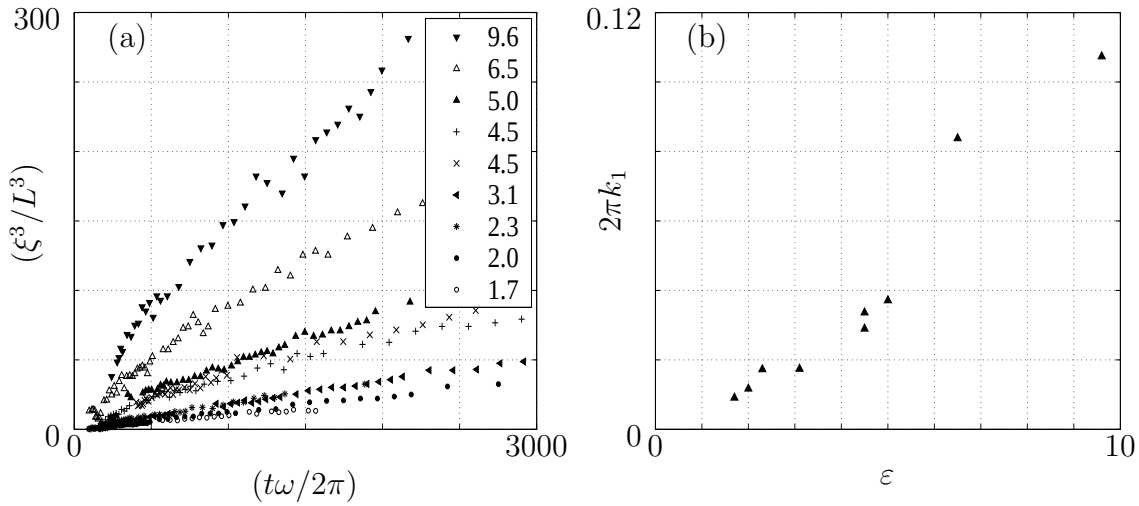

Fig. 9. (a) (ξ^3/L^3), with $L = R_d(\Omega/N_0)^{\frac{2}{3}}$, plotted against number of disk rotations, $n = \omega t/2\pi$, for each of the experiments listed in Table 1; the corresponding values of Rossby number, ε, are given in the legend. (b) Corresponding estimates for the proportionality coefficient $k_1(\varepsilon)$ obtained from each of the scaled data using a least-squares linear fit.

the influence of background rotation must eventually become important once more in the controlling flow dynamics, albeit initially remaining a secondary factor relative to the motions induced by the disk. The growth rate of $\xi(r,t)$ during this intermediate stage will be represented by a scaling of the form (9) based on the relevant scales $(R_d\omega, R_d\Omega, \omega^{-1})$, with corresponding L given by,

$$L = R_d\left(\omega\Omega/N_0^2\right)^{\frac{1}{3}} = R_d\left(\lambda_1\lambda_2\right)^{-\frac{1}{3}}. \tag{12}$$

The data shown in Fig. 9 were also plotted using the scaling represented by (9) and (12). For $\varepsilon > 4$ the data were found to accord well with this scaling. However, for the lower range values of Rossby number the monotonic relationship between k_1 and ε was lost, indicating that these data were not consistent with this model.

Although not directly relevant to the experiments presented in this article, it is also illuminating to briefly discuss how the model for the interface growth rate will behave when $\varepsilon \to 0$ by considering the limit $\omega \to 0$ where, similarly, Ω is kept fixed. As $\omega \to 0$, the motions induced by the disk rotation become secondary and the growth rate of $\xi_1(r,t)$ is dominated by the secondary flow induced by the boundary layer adjacent to the disk surface, which can be characterized by respective radial and vertical velocity scales $\left(R_d\Omega, (\nu\Omega)^{\frac{1}{2}}\right)$ (Greenspan, 1965). In this case, the rate of input work can be expressed as,

$$\frac{\mathrm{d}}{\mathrm{d}t}W_2 \sim \rho(\nu\Omega)^{\frac{1}{2}}\Omega^2 R_d^4. \tag{13}$$

Again, assuming that a proportion of this work is used to mix the fluid within

the interfacial volume, (6) combined with (13) gives,

$$\left(\xi^3/L^3\right) \sim t/\tau, \tag{14}$$

where $\tau = N_0^{-1} E^{-\frac{1}{2}}$ and,

$$L = R_d (h/R_d)^{\frac{1}{3}} \Omega/N_0 = R_d\, \eta^{-\frac{1}{3}} \lambda_1^{-1} = l_z\, \eta^{-\frac{1}{3}}, \tag{15}$$

the length-scale l_z identified by Moulin & Flór (2004).

5 Discussion

The laboratory measurements and flow visualization data have shown that the presence of background rotation affects significantly the structure of the three-dimensional circulation and density field deformation induced by the rotation of a horizontal disk in a stable, linearly-stratified fluid. Though many of the features of the flow - for example, the generation of a mixed layer adjacent to the disk, the vertical growth of the mixed layer with time and the formation of density interfaces - are qualitatively similar to those observed in the non-rotating case (Davies *et al.*, 1995), the dynamics of the flow development are dominated by the Ekman processes associated with the background rotation, even for cases in which the Rossby number of the flow is order unity or greater. In particular, the results demonstrate that energy-based scalings developed previously for the growth with time of the mixed layer thickness in the non-rotating frame are invalid in the rotating frame. When Ekman suction processes associated with the background rotation are considered, the resulting scaling predictions for the growth of the mixed layer are shown to accord well with the laboratory data, with the parametric dependence of the layer thickness showing a systematic dependence upon the Rossby number that is consistent with the growing dominance of background rotation as the Rossby number decreases. The transition between flows that are relatively dominated and insensitive respectively to background rotation has been treated successfully in the data analysis by suitable choice of the normalizing length scales for the $\varepsilon \sim \mathcal{O}(1)$ and $\varepsilon > \mathcal{O}(1)$ flows, with consistency being demonstrated between these and the counterpart scalings (Davies *et al.*, 1995) for the limiting case $\varepsilon \to \infty$ appropriate for flows with no background rotation.

To enable direct comparisons with the previous related investigation by (Davies *et al.*, 1995), the present paper has focussed upon cases for which the fluid system is strongly forced, with the value of the disk Reynolds number being sufficiently high for the flow to be turbulent in the early stages of development and for forcing to generate initially a mixed layer close to the disk. As with the counterpart cases studied by Davies *et al.* (1995) for the non-rotating

configuration, the value of Reynolds number $Re = \omega R_d^2/\nu = 2\varepsilon\eta^2/E$ is also assumed to be sufficiently high for Reynolds number effects to be neglected. The significantly different flow regimes characteristic of weak forcing (i.e relatively low values of Re and ε) are not considered here and are the subject of another study.

Acknowledgments

This work was supported by the EPSRC, grant number GR/R74703/01, under the Physics-Engineering Programme.

References

Barcilon, V. and Pedlosky, J., 1967. On the steady motions produced by a stable stratification in a rapidly rotating fluid. *J. Fluid Mech.*, **29**, 673–690.

Boyer, D. L., Davies, P. A. and Guo, Y., 1997. Mixing of a two-layer stratified fluid by a rotating disk. *Fluid Dyn. Res.*, **21**, 381-401.

Chai, A. and Kit, E., 1991. Experiments on entrainment in an annulus with and without velocity gradient across the density interface. *Exp. Fluids*, **11**, 45-57.

Chai, A., Tanny J. and Kit, E., 1993. Experimental investigation of turbulent entrainment in an annulus with moving sidewalls. *Exp. Fluids*, **15**, 97-107.

Davies, P. A., 1992. Aspects of flow visualization and density field monitoring of stratified flows. *Optics and Lasers in Eng.*, **16**, 311–335.

Davies, P. A., Guo, Y., Boyer, D. L. and Folkard, A. M., 1995. The flow generated by the rotation of a horizontal disk in a stratified fluid. *Fluid Dyn. Res.*, **17**, 27–47.

Ekman, V. W., 1905. On the influence of the earth's rotation on ocean-currents. *Ark. Mat. Astr. Fys.*, **2**, 1–52.

Endoh, S., Okamoto, I. and Okumura, Y., 1990. Recent study on water movement in Lake Biwa. *Japan Journal of Limnology*, **51**, 25-26.

Fernando, H. J. S., 1991. Turbulent mixing in stratified fluids. *Annu. Rev. Fluid Mech.*, 23, 455-493.

Folse, R. F., Rodrigue, D. A. and Courtney, D. L., 1986. Measurements of the size of the secondary flow regions generated by a torsionally oscillating disk in linearly stratified fluid. *Phys. Fluids*, **29**(3), 667-671.

Folse, R. F. and Wu, X., 1989. Ekman number dependence of the size of secondary flow regions generated by torsionally oscillating disks in stratified fluids. *Phys. Fluids (A)*, **1**(5), 892-894.

Fortuin, J. M. H., 1960. Theory and application of two supplementary methods

of constructing density gradient columns. *Journal of Polymer Science*, **44**, 505-515.

Greenspan, H. P., 1968. *The Theory of Rotating Fluids.* Cambridge University Press.

Head, M. J., 1983. The use of four-electrode conductivity probes for high resolution measurement of turbulent density or temperature variation in salt-stratified water flows. PhD dissertation, University of California, San Diego.

Kantha, L. H., Phillips, O. M. and Azad, R. S., 1977. On turbulent entrainment at a stable density interface. *J. Fluid Mech.*, **79**, 753-768.

Kato, H. and Phillips, O. M., 1969. On the penetration of a turbulent layer into a stratified fluid. *J. Fluid Mech.*, **37**, 643-655.

Moulin, F. Y. and Flór, J.-B., 2004. On the spin-up by a rotating disk in a rotating stratified fluid. *J. Fluid Mech.*, **516**, 155–180.

Scranton, D. R. and Lindberg W. R., 1983. An experimental study of entraining, stress-driven stratified flow in an annulus. *Phys. Fluids*, **26**(5), 1198-1205.

Shankar, P. N. and Deshpande, M. D., 2000. Fluid mechanics in the driven cavity. *Annu. Rev. Fluid Mech.*, **32**, 93-136.

Spence, G. S., Foster, M. R. and Davies, P. A., 1992. The transient response of a contained rotating stratified fluid to impulsively started surface forcing. *J. Fluid Mech.*, **243**, 33–50.

Turner J. S., 1973. *Buoyancy Effects in Fluids (2nd ed)*, Cambridge University Press, Cambridge, UK.

Walin, G., 1969. Some aspects of time-dependent motion of a stratified rotating fluid. *J. Fluid Mech.*, **36**, 289–307.